Int J Adv Manuf Technol (2015) 81:875–885
DOI 10.1007/s00170-015-7282-0

ORIGINAL ARTICLE

A grinding force model for ultrasonic assisted internal grinding (UAIG) of SiC ceramics

Jianguo Cao[1] · **Yongbo Wu**[2] · **Jianyong Li**[1] · **Qinjian Zhang**[1]

Received: 21 November 2014 / Accepted: 4 May 2015 / Published online: 14 May 2015

Abstract As grinding force plays an influential role in work-surface finish in grinding process, a model is necessary for optimizing input variables to achieve high product quality and productivity. However, to the best of our knowledge, there are few reports on modeling grinding force in ultrasonic assisted internal grinding (UAIG). In this study, a theoretical model is presented to predict the grinding force in UAIG of SiC ceramics. This model stems from undeformed chip length resulting from the relative motion between the grinding wheel and the workpiece. After analyzing the cutting action of an active individual grain, normal and tangential force models for the UAIG of SiC ceramics are developed. Using the developed model, the influence of many principal input variables, namely the workpiece rotational speed n_w, the wheel infeed rate V_c, the wheel rotational speed n_g, the UV amplitude A_u, and the oscillation frequency f_o, on grinding force is predicted. Comparing the predicted forces with the experimental ones, it is shown that the predicted forces agree reasonably well with the experimental ones. The obtained results show that (1) the grinding forces are reduced in the UAIG compared to conventional internal grinding, which is attributed to the formation of the longer undeformed chip length in the UAIG; (2) the influence of n_g, n_w, and V_c on grinding force are much pronounced, whereas that of A_u and f_o are not very noticeable; and (3) the force reduction of UV can be enhanced either by decreasing n_g, n_w, and V_c or increasing A_u and f_o.

Keywords Grinding force · Ultrasonic vibration · Internal grinding · SiC ceramics · UAIG

1 Introduction

In recent years, mechanical components with precision internal cylindrical surface have been widely used in various engineering applications, such as injection nozzles for automotive engine, inner or/and outer races of bearings, and sleeve of ceramics mold for hot press molding of glass lenses. Up to the present day, internal grinding has been employed as the major method for machining the internal surface of these components, especially for those made of ceramics. However, there are some disadvantages in conventional internal grinding (CIG) [1]: an ultra-high-speed grinding spindle with rotational speed of up to 200,000 rpm should be installed on the internal grinder to improve the surface quality and ensure the form/dimensional accuracy, leading to an inevitable huge cost; as the spindle rotates at an ultra-high speed, the bearings will easily get heating and the spindle will generate vibration easily, resulting in difficulty in obtaining high finishing accuracy; the contact arc length between grinding wheel and workpiece is longer than that in cylindrical or surface grinding, easily resulting in heavy loading of grinding wheel, subsequently grinding wheels with coarse grits should be employed to prevent the wheel from loading but in turn a high accuracy finishing surface is difficult to attain. Therefore, a new machining method is required for the high precision and efficient processing of internal cylindrical surfaces.

Ultrasonic assisted grinding (UAG), a hybrid machining process combining grinding and ultrasonic vibration (UV), can increase the grinding efficiency and improve the grinding quality due to the reductions in grinding forces and wheel wear for the sake of UV [2–4]. By getting the benefit of UV, UAG technique has been introduced into the internal grinding to perform the ultrasonic assisted internal grinding (UAIG) of

✉ Yongbo Wu
wuyb@akita-pu.ac.jp

[1] School of Mechanical, Electronic and Control Engineering, Beijing Jiaotong University, Beijing 100044, People's Republic of China

[2] Department of Machine Intelligence and Systems Engineering, Akita Prefectural University, Yurihonjo, Akita 015-0055, Japan

difficult-to-machine materials. Kumabe and Ito [5] applied the UV to internal grinding to perform ultrasonic assisted internal grinding (UAIG) of metal materials such as aluminum, copper and steel. The obtained results showed that the grinding efficiency was improved and grinding forces were reduced for the sake of the presence of UV. Wu et al. [6] found that the normal and tangential forces in UAIG of stainless steel were smaller by 65 and 70 %, respectively, and the surface roughness was smaller by 20 % than those in CIG. In the study of Fujimoto et al. [7], the machining characteristics of the UAIG of tungsten were experimentally compared with those of the CIG, showing that the normal and tangential grinding forces and the surface roughness in UAIG were smaller by 11, 41, and 53 %, respectively, than those in CIG. In our previous study, the machining characteristics of UAIG of SiC ceramics were observed [8]. The results showed that the normal and tangential grinding force in UAIG are significantly reduced compared with those in CIG; the greater improvement of the form accuracy and the surface roughness are achieved in UAIG compared with those in CIG .

In general, the grinding force plays an important role in grinding process as it not only has a direct influence on the wheel wear, grinding accuracy, grinding temperature, and surface integrity but also strongly affects the material removal mechanism [9]. As for the influence of the UV on the grinding force, until now many studies have been concentrated on discussing the grinding force in UAG, and several grinding force models have been developed for UAG. Nomura et al. [10] developed a grinding force model for UAG by analyzing the grinding wheel-workpiece contact length and discussing the underformed chip cross-sectional area. Shimada et al. [11] also developed a force model for UAG by discussing the underformed chip cross-sectional area after analyzing the relative velocity between the grain and the workpiece. Qin et al. [12] proposed a grinding force model for the UAG of titanium and subsequently revealed that the tool is not in continuous contact with the workpiece and the interaction between a diamond grain, and the workpiece is considered as a penetration process, followed by establishing the relationship between the grinding force and the input variables. Wang et al. [13] proposed a UAG grinding force model based on the average chip cross-sectional area theory and found that grinding force decreases because of the UAG average chip cross area is smaller than conventional grinding. Although some grinding force models for UAG were established so far as mentioned above, the effect of UV parameters on grinding force has not been analyzed. Furthermore, no publication is available on grinding force model for UAIG.

In this study, in order to help understanding the material removal mechanism and optimizing the input variables (the workpiece rotational speed n_w, the wheel infeed rate V_c, the wheel rotational speed n_g, the UV amplitude A_u, and the oscillation frequency f_o, etc.) in the UAIG of SiC ceramics, a grinding force model to predict relations between grinding force and input variables is developed after analyzing the relative motion between the grinding wheel and the workpiece. In addition, expressions for the normal and tangential grinding forces in UAIG are established by analyzing the cutting process of an active individual abrasive grain participating in grinding. In this study, at first, the model development approach is described in details. Afterwards, using the developed model, influences of the input variables on the grinding force are predicted. Finally, predicted results are compared with experimentally obtained ones to confirm the validity of the developed model.

2 Processing principle of UAIG and model development approach

2.1 Processing principle of UAIG

Figure 1 schematically illustrates the processing principle of UAIG. The grinding wheel rotates at a rotational speed of n_g and ultrasonically vibrates along its axis at frequency of f_u and amplitude of A_u. In the meanwhile, the wheel is fed in its radial direction toward the internal surface of the workpiece at an infeed rate of V_c, and the workpiece rotates at a rotational speed of n_w. In addition, an oscillation motion is given to the grinding wheel at a frequency of f_o and a stroke of A_o along the wheel axis in order to expand the machining area and improve the work-surface quality.

2.2 Model development approach

As a combination of grinding and UV, there are a number of input variables in UAIG process as shown in Table 1. Usually, the macroscopic results are composed of the microscopic effects, especially the cutting action in grinding is the summation of the microscopic effects of all individual abrasive grains. Many grinding force models were established for surface grinding by analyzing an active individual abrasive grain that participates in cutting and summing up the effects of all active abrasive particles [14, 15]. A similar approach is also used in the present work to develop the force model for UAIG. As shown in Fig. 2, the model development steps are as follows:

1. Establish a relationship between input variables and undeformed chip cross-sectional area A_{cs}.
2. Calculate the undeformed chip length $L_{c\text{-}UAIG}$ by considering the relative motion between the grinding wheel and the workpiece in UAIG.
3. Analyze the cutting process of an active individual abrasive grain participating in grinding action and establish the tangential force and normal force model, f_t and f_n, for an individual abrasive grain.
4. Establish the grinding force model, i.e., the tangential force and normal force model, $F_{n\text{-}UAIG}$ and $F_{t\text{-}UAIG}$, for

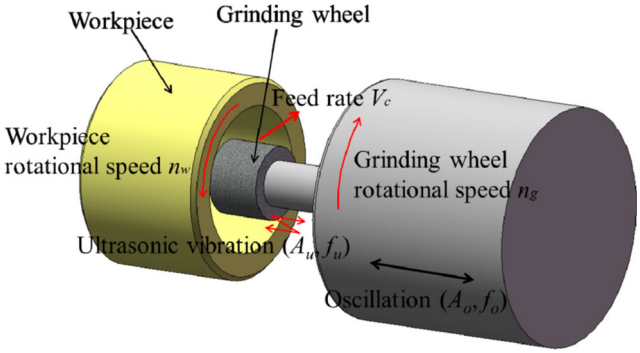

Fig. 1 Schematic illustration of the processing principle of UAIG

UAIG process by aggregating the effects of all active abrasive grains.

3 Model development details

The complete description of grinding process is very difficult due to the complex cutting behavior of abrasive grains. Thus, prior to developing the model in details the major assumptions and simplifications are given as follows:

1. All abrasive grains on grinding wheel are rigid.
2. Abrasive grains located on the grinding wheel surface have the same height, and all of them take part in cutting in the grinding process.
3. Elastic/heat deflection between the grinding wheel and the workpiece and uneven distribution of the grains on the peripheral surface of the wheel are ignored.

3.1 Undeformed chip cross-sectional area

In grinding, the total volume of the chips formed per unit time, V_{chip}, is the ensemble of the volumes formed by all individual active grains in the grinding zone per unit time. Consequently, the V_{chip} can be calculated from the average cross-sectional area A_{cs} and length L_c of the undeformed chip and the number of active cutting grains in the grinding zone per unit time N_d as follows:

$$V_{chip} = N_d A_{cs} L_c \tag{1}$$

Letting the active cutting edge density, the grinding width and the grinding wheel peripheral speed be c_d, b and V_g, respectively, gives

$$N_d = c_d b V_g. \tag{2}$$

On the other hand, the removed material per unit time, W_m, by the wheel can be written as

$$W_m = 2\pi a_e R_w b n_w \tag{3}$$

where a_e, R_w, and n_w are the wheel depth of cut, the workpiece internal radius, and the workpiece rotational speed, respectively.

In internal grinding, the V_{chip} is supposed to be equal to the W_{m}, resulting in a relationship as expressed as follows:

$$N_d A_{cs} L_c = 2\pi a_e R_w b n_w \tag{4}$$

Substituting Eq. (2) into Eq. (4) followed by rearranging yields the average undeformed chip cross-sectional area A_{cs} as follows:

$$A_{cs} = 2\pi a_e R_w n_w \Big/ c_d V_g L_c = a_e R_w n_w \Big/ c_d R_g n_g L_c \tag{5}$$

where R_{g} and n_g are the radius and rotational speed of the grinding wheel, respectively.

3.2 The undeformed chip length

Figure 3 shows the geometrical arrangement between the grinding wheel and the workpiece and the relative motion of the grinding wheel to the workpiece during UAIG. The symbols a and R_{w0} stand for the distance between the centers of the workpiece and the grinding wheel at grinding start point and the initial radius of workpiece before grinding, respectively. Let a xyz-coordinate system be fixed on the workpiece; the x-axis is along the grinding wheel infeed direction, the y-axis is perpendicular to the wheel infeed direction, and the z-axis is along the workpiece axis. The origin point o is fixed at the center of the workpiece. It can be seen from the figure that in the UAIG, the grinding wheel has five different relative motions to the workpiece, i.e., a infeed motion in x-axis at the

Table 1 Input variables in UAIG process

Grinding wheel variables	Workpiece variables	UV variables	Grinding process parameters
Wheel width, b	Workpiece radius, R_w	Amplitude, A_u	Infeed rate, V_c
Wheel radius, R_g	Workpiece rotational speed, n_g	Frequency, f_u	Depth of cut, a_e
Wheel rotational speed, n_g			Oscillation stroke, A_o
			Oscillation frequency, f_o

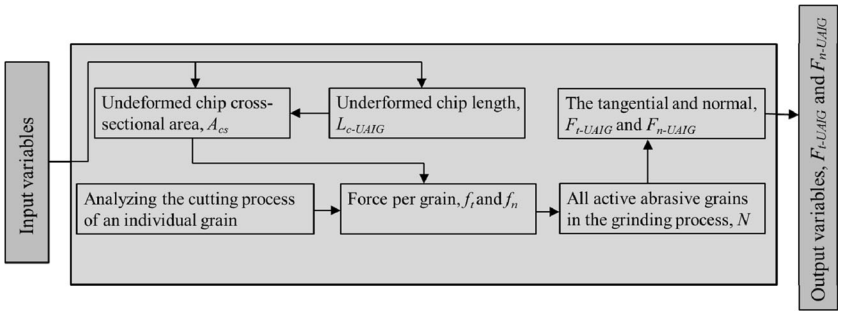

Fig. 2 Development process of the grinding force model for UAIG

infeed rate of V_c, a rotation around its own axis at the speed of n_g, a revolution motion around z-axis at the speed of n_w, a UV in z-axis at the frequency of f_u and the amplitude of A_u, and an oscillation in z-axis at the frequency of f_o and the stroke of A_o. It can be figured out that owing to the spiral relative motion of the wheel to the workpiece caused by the simultaneous presence of the wheel infeed motion and the workpiece rotation motion (i.e., the wheel revolution motion around z-axis), the profile of the workpiece internal surface would be shaped to be spiral as shown in Fig. 3a.

Under the presence of the five relative motions, the instant geometrical relationship between the workpiece and the grinding wheel at grinding time t_0, i.e., after grinding for time t_0 is supposed to be as shown in Fig. 4. Let an abrasive grain G be at the point P_0 at time t_0 when it takes part in the cutting action. Then, after the grinding is further performed for time ΔT ($=t_1 - t_0$), the abrasive grain G gets out of the cutting action at the point P_1. ΔT can be obtained by Eq. (6) from the geometrical relationship shown in Fig. 4:

$$\Delta T = l_c \Big/ 2\pi n_g R_g \tag{6}$$

where l_c is the grinding wheel-workpiece contact length (Fig. 4), which can be written as follows [15]:

$$l_c = \sqrt{D_e a_e} \tag{7}$$

D_e is the equivalent wheel diameter, which can be expressed as

$$D_e = \frac{2R_g}{1 - R_g \Big/ R_w(t)} \tag{8}$$

where $R_w(t)$ is the radius of workpiece in the grinding process at time t, $R_w(t)=R_{w0}+V_c t$.

As the abrasive grain G is at the point P_0 ($x= a+R_g+V_c t_0$, $y=0$, $z=0$) at time t_0 when it takes part in the cutting action, then at time t ($t_0 \le t \le t_1$) its coordinates are obtained as Eq. (9) from the geometrical relationship shown in Fig. 4.

$$\begin{cases} x = a + V_c t + R_g \cos\left(2\pi n_g (t - t_0)\right) \\ y = (a + V_c t)\cos(2\pi n_w (t - t_0)) + R_g \sin\left(2\pi n_g (t - t_0)\right) \\ z = A_u \sin(2\pi f_u (t - t_0)) + A_o \sin(2\pi f_o (t - t_0)) \end{cases} \tag{9}$$

Differentiating Eq. (9) with respect to t, gives

$$\begin{cases} dx = \left[V_c - 2\pi R_g n_g \sin\left(2\pi n_g (t - t_0)\right)\right] dt \\ dy = V_c \cos(2\pi n_w (t - t_0)) - 2\pi n_w (a + V_c t)\sin(2\pi n_w (t - t_0)) + 2\pi n_g R_g \cos\left(2\pi n_g (t - t_0)\right) \\ dz = 2\pi \left[A_u f_u \cos(2\pi f_u (t - t_0)) + A_o f_o \cos(2\pi f_o (t - t_0))\right] dt \end{cases} \tag{10}$$

Subsequently, the undeformed chip length in UAIG $L_{c\text{-}UAIG}$ can be determined by the following equation.

$$\begin{aligned} L_{c-UAIG} &= \int_{t_0}^{t_0+\Delta t} \sqrt{dx^2 + dy^2 + dz^2}\, dt \\ &= \int_{t_0}^{t_0+\Delta t} \sqrt{\begin{array}{l} \left[V_c - 2\pi R_g n_g \sin\left(2\pi n_g (t - t_0)\right)\right]^2 \\ + \left[V_c \cos(2\pi n_w (t - t_0)) - 2\pi n_w (a + V_c t)\sin(2\pi n_w (t - t_0)) + 2\pi n_g R_g \cos\left(2\pi n_g (t - t_0)\right)\right]^2 \\ + 4\pi^2 \left[A_u f_u \cos(2\pi f_u (t - t_0)) + A_o f_o \cos(2\pi f_o (t - t_0))\right]^2 \end{array}} dt \end{aligned} \tag{11}$$

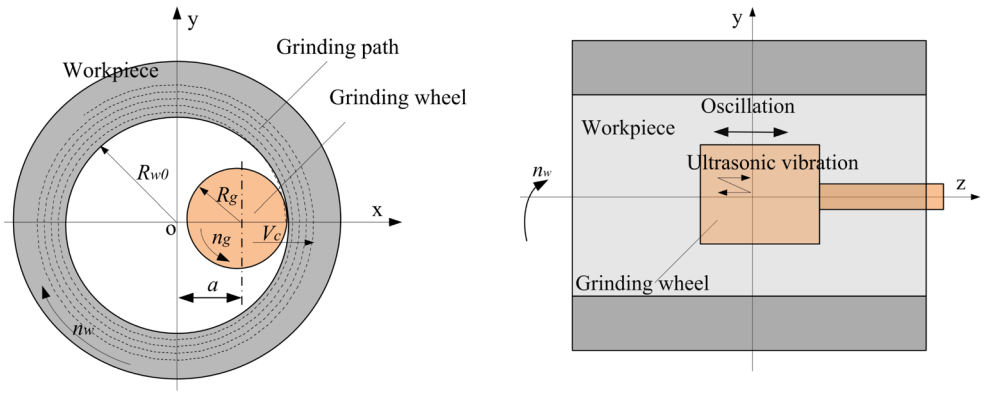

Fig. 3 Geometrical arrangement between grinding wheel and workpiece

The CIG process can be considered as a special case of UAIG process when A_u=0. Thus, the undeformed chip length in CIG $L_{c\text{-}CIG}$ can be obtained by substituting A_u=0 into Eq. (11).

3.3 The force model

Figure 5a shows a simplified cutting force model for a single abrasive grain in UAIG. The tangential and normal cutting forces, f_t and f_n, acting on the grain can be determined as the function of the undeformed chip cross-sectional area A_{cs} [15], i.e.,

$$f_n = kA_{cs} \tag{12}$$

$$f_t = k_1 kA_{cs} \tag{13}$$

where k is the chip thickness coefficient, and k_1 is the ratio of the tangential force to the normal force.

As the ultrasonic vibration period is extremely small compared with the oscillation period, sinusoidal cutting traces of abrasive grains can be hence approximately generated on the work surface in UAIG as shown in Fig. 5b. This means that the direction of the tangential force f_t varies in a sinusoidal pattern and the f_t can be separated into two components along y- and z-axes, respectively, i.e., f_y and f_z (Fig. 5b), as follows:

$$\begin{cases} f_y = f_t \cos\theta \\ f_z = f_t \sin\theta \end{cases} \tag{14}$$

where θ is the engagement angle and given by

$$\theta = \tan^{-1}\left(V_z(t)\Big/V_y(t)\right) = \tan^{-1}\left(dz\Big/dy\right) \tag{15}$$

where $V_y(t)$ and $V_z(t)$ are velocities in y- and z-axes, respectively, which can be obtained by Eq. (10). Subsequently, the θ can be determined by substituting Eq. (10) into Eq. (15). For

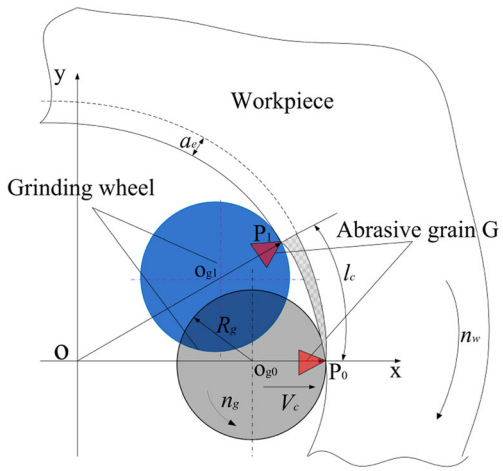

Fig. 4 Relative motion between the grinding wheel and the workpiece

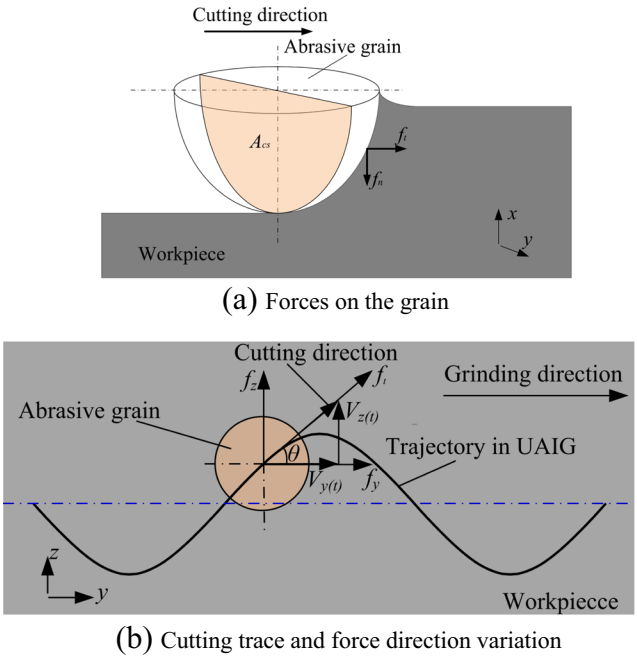

Fig. 5 Simplified cutting force model for a single abrasive grain in UAIG

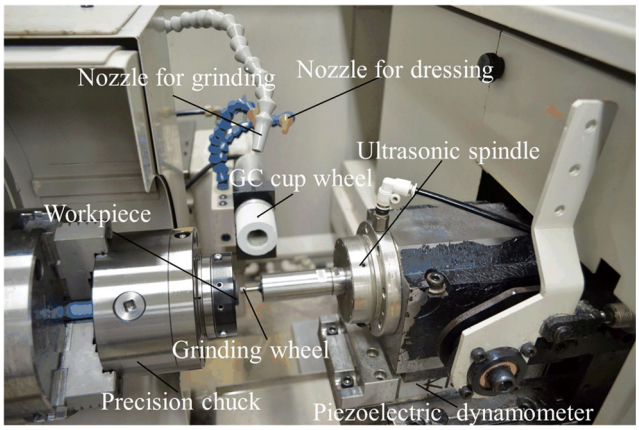

Fig. 6 Experiment setup for UAIG

instance, under the input variables of n_w=300 rpm, n_g= 4000 rpm, V_c=10 μm/min, A_u=4 μm, f_u=40 kHz, A_o= 4 mm, f_o=0.625Hz, and in one UV period, the θ would be in the range of [−50.2°, 50.2°] according to Eq. (15).

It is deduced from Eqs. (14) and (15) that the force f_z periodically changes in z-direction within the certain range of θ, resulting in the mean force f_z in one UV period being almost zero. Therefore, hereafter, only the forces in x- and y--directions, i.e., tangential and normal forces, are considered.

As mentioned above, the forces in x- and y-directions are fluctuating periodically. It is helpful for dealing with the fluctuating forces to introduce the average value of the fluctuating one. In addition, the resultant grinding forces acting on the grinding wheel are the sum of the forces acting on all active grains within the grinding zone. Following the calculation method of the average force [16], the average value of the normal force and the tangential force, $F_{n\text{-}UAIG}$ and $F_{t\text{-}UAIG}$, during the time period $\Delta t(=t_1-t_0)$ in UAIG, can be written as

$$\begin{cases} F_{t-UAIG} = N\dfrac{1}{\Delta t}\displaystyle\int_{t_0}^{t_0+\Delta t} f_y dt = Nk_1kA_{cs}\dfrac{1}{\Delta t}\int_{t_0}^{t_0+\Delta t}\cos\theta dt \\ F_{n-UAIG} = N\dfrac{1}{\Delta t}\displaystyle\int_{t_0}^{t_0+\Delta t} f_x dt = NkA_{cs} \end{cases} \tag{16}$$

Table 2 Experimental conditions for obtaining k and k_1

Test no.	n_g (rpm)	n_w (rpm)	A_u (μm)	V_c (μm/min)
1	4000	300	4	10
2	4000	200	4	10
3	5000	300	4	10
4	4000	300	3	10
5	4000	300	4	15

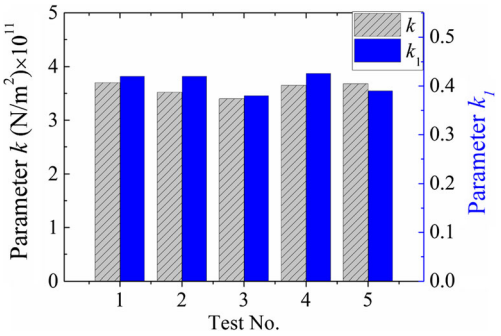

Fig. 7 Value of k and k_1 obtained in all of the tests

where N is the total number of active cutting edges in grinding zone and can be obtained with Eq. (17) [17]:

$$N = c_d b l_c \tag{17}$$

where l_c is the grinding wheel-workpiece contact length which can be determined with Eq. (18) [15]:

$$l_c = \sqrt{\frac{2R_g a_e}{1-R_g/R_w(t)}} \tag{18}$$

By substituting Eqs. (5), (12–15), (17), and (18) into Eq. (16), the normal force and the tangential force, $F_{n\text{-}UAIG}$ and $F_{t\text{-}UAIG}$, at time t_0, can be written as

$$\begin{cases} F_{t-UAIG} = k_1 k\sqrt{\dfrac{2R_g a_e}{1-R_g/(R_{w0}+V_c t_0)}\dfrac{b(R_{w0}+V_c t_0)a_e n_w}{R_g n_g L_{c-UAIG}}}\dfrac{1}{\Delta t}\displaystyle\int_{t_0}^{t_0+\Delta t}\cos\theta dt \\ F_{n-UAIG} = k\sqrt{\dfrac{2R_g a_e}{1-R_g/(R_{w0}+V_c t_0)}\dfrac{b(R_{w0}+V_c t_0)a_e n_w}{R_g n_g L_{c-UAIG}}} \end{cases} \tag{19}$$

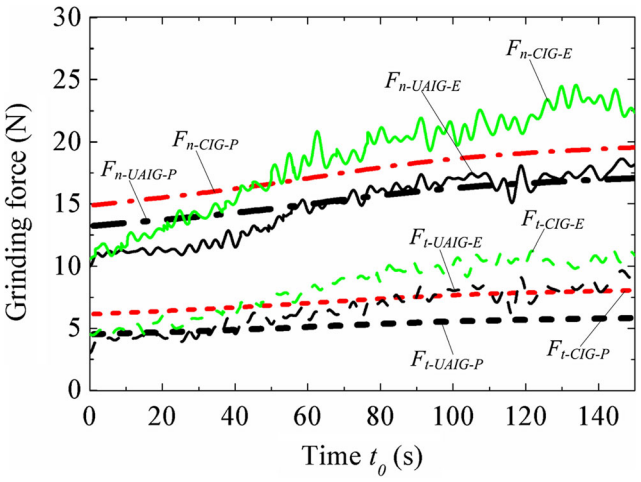

Fig. 8 Grinding forces versus time t_0 in UAIG and CIG tests

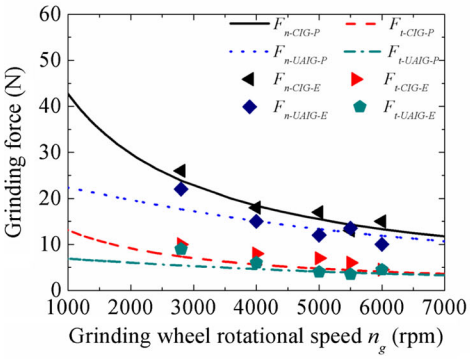

(a) Influence of grinding wheel rotational speed n_g (n_w=300rpm, V_c=10μm/min, A_u=4μm, f_o=0.625Hz)

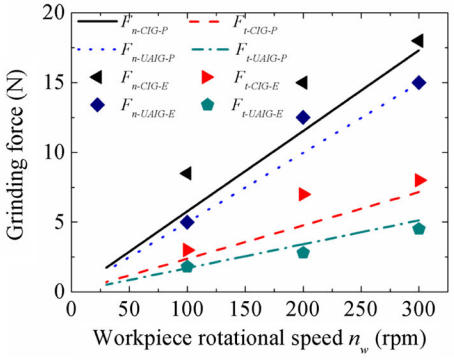

(b) Influence of workpiece rotational speed n_w (n_g=4000rpm, V_c=10μm/min, A_u=4μm, f_o=0.625Hz)

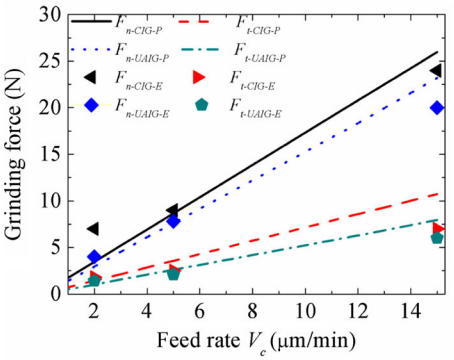

(c) Influence of feed rate V_c (n_g=4000rpm, n_w=300rpm, A_u=4μm, f_o=0.625Hz)

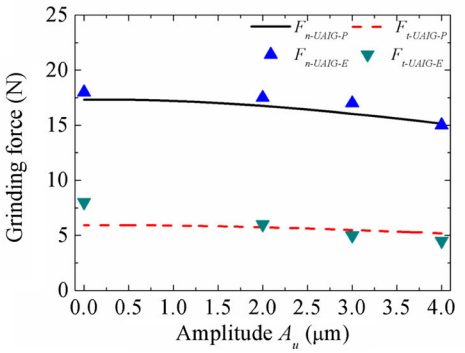

(d) Influence of UV amplitude A_u (n_g=4000rpm, n_w=300rpm, V_c=10μm/min, f_o=0.625Hz)

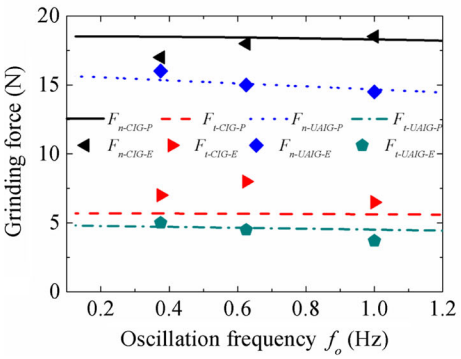

(e) Influence of oscillation frequency (n_g=4000rpm, n_w=300rpm, A_u=4μm, V_c=10μm/min)

Fig. 9 Relations between grinding forces and process parameters

where $L_{c\text{-}UAIG}$ can be obtained by Eq. (11). As mentioned above, the CIG process is a special case of UAIG process with A_u=0, hence θ=0°. Thus, the tangential force $F_{t\text{-}CIG}$ and the normal force $F_{n\text{-}CIG}$ in CIG can be obtained by substituting A_u=0 and θ=0 into Eq. (19), gives.

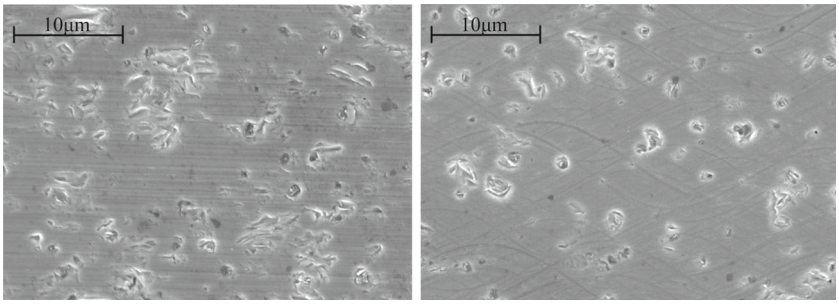

Fig. 10 SEM images of work surface by CIG and UAIG

(a) Work-surface finished by CIG (b) Work-surface finished by UAIG

$$\begin{cases} F_{t-CIG} = k_1 k \sqrt{\dfrac{2R_g a_e}{1-R_g \Big/ (R_{w0}+V_c t_0)} \dfrac{b(R_{w0}+V_c t_0) a_e n_w}{R_g n_g L_{c-CIG}}} \\ F_{n-CIG} = k \sqrt{\dfrac{2R_g a_e}{1-R_g \Big/ (R_{w0}+V_c t_0)} \dfrac{b(R_{w0}+V_c t_0) a_e n_w}{R_g n_g L_{c-CIG}}} \end{cases} \tag{20}$$

3.4 Experimental determination of parameters k and k_1

According to Eq. (19) and (20), it is essential to determine the actual values of the chip thickness coefficient, k, and the ratio of the tangential force to the normal force, k_1, to predict the grinding forces quantitatively. For this purpose, UAIG experiments were performed involving a SiC ceramics workpiece of φ12mm in inner diameter, φ22mm in outer diameter and 13 mm in thickness for measuring the grinding forces under various input variables. Figure 6 shows a photograph of the experimental setup constructed in-house by installing an ultrasonic spindle (URT40 by Takesho Co., Ltd.) on an existing NC internal grinder (GRIND-X IGM15EX by Okamoto Machine Tool Works, Ltd.) via a three-component piezoelectric dynamometer (9256A by Kistler Co., Ltd.). A metal-bonded diamond grinding wheel (SD3000P100M, φ6×t5mm) was screwed onto the end face of the ultrasonic spindle and rotated together with the rotation of the spindle. A rotary dresser attached with a GC cup wheel was used for the truing/dressing of the grinding wheel. During grinding, coolant (solution type, 1.6 % dilution) was supplied into the grinding zone.

Although the k and k_1 are independent of the input variables and hence their values can be determined by only one round of grinding test under a certain set of input variables in principle, five rounds of grinding tests were performed under different sets of input variables as shown in Table 2 and the average of five data obtained either for the k or for the k_1 was adopted to indicate the k or the k_1 in order to avoid the deviation due to the input variables. In the current work, the other input variables are kept constant at f_u=40 kHz, A_o=4 mm, f_o=0.625Hz, R_{w0}=6 mm, R_g=3 mm, b=5 mm, $a_e=V_c/n_w$, and radial stock removal of 25 μm.

In each test, the corresponding grinding forces, $F_{n\text{-}UAIG}$ and $F_{t\text{-}UAIG}$, were obtained. Substituting the obtained values of $F_{n\text{-}UAIG}$ and $F_{t\text{-}UAIG}$ and all input variables (t_0=75 s) into Eq. (19) followed by re-ranging yielded the values of k and k_1. Figure 7 shows the values of k and k_1 obtained in all of the tests. It can be figured out that there are not strong correlations between the input variables and the values of k and k_1, and the average values of k and k_1 were 3.58×10^{11}(N/m^2) and 0.413, respectively. Consequently, in the present work, the grinding forces in UAIG and CIG at time t_0 can obtained by substituting k=3.58×10^{11}(N/m^2) and k_1=0.413 into Eqs. (19) and (20), respectively.

4 Grinding forces predictions and model verification

To verify the grinding force model, CIG and UAIG tests under the input variables of n_w=300 rpm, n_g=4000 rpm, V_c=10 μm/min, A_u=0/4 μm, f_u=40 kHz, A_o=4 mm, and f_o=0.625Hz were performed and the forces prediction was also carried out under the same input variables using Eqs. (19) and (20) for comparison. The experimentally obtained and predicted variations of the grinding forces during grinding are plotted in Fig. 8 (the subscripts -P and -E stand for the predicted force and the experimental one, respectively). Comparing the predicted forces with the experimental ones shows that although there are somewhat quantitative differences between them which is probably caused by the lack of the inclusion of some input variables, e.g., coolant and wheel loading in the development of grinding force model, the variation tendencies and the quantitative values of the predicted forces agree reasonably with those of the experimental ones, both in CIG and in UAIG process. This fact validated the developed force model. It is also found from Fig. 8 that the grinding forces increase with the increasing of the grinding time t_0 both in CIG and UAIG within the tested grinding period in the current grinding conditions.

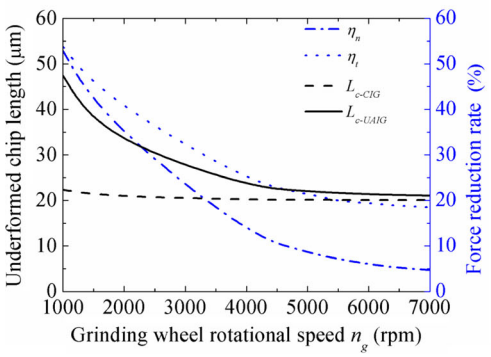

(a) Influence of grinding wheel rotational speed n_g.
(n_w=300rpm, V_c=10μm/min, A_u=4μm, f_o=0.625Hz)

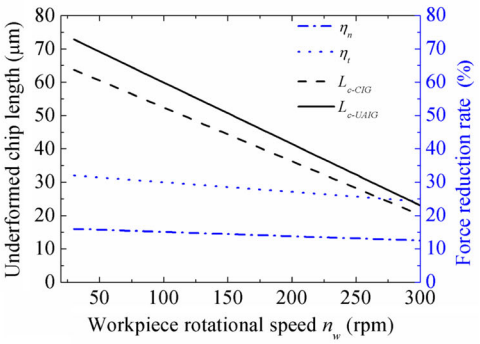

(b) Influence of workpiece rotational speed n_w.
(n_g=4000rpm, V_c=10μm/min, A_u=4μm, f_o=0.625Hz)

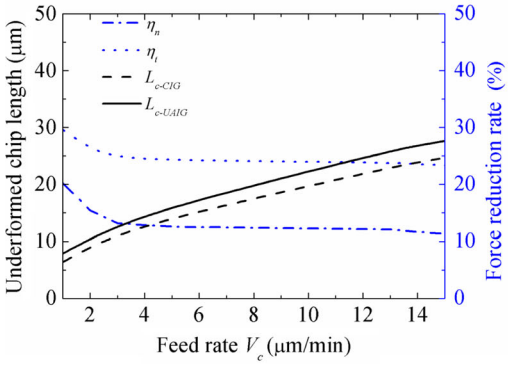

(c) Influence of feed rate V_c
(n_g=4000rpm, n_w=300rpm, A_u=4μm, f_o=0.625Hz)

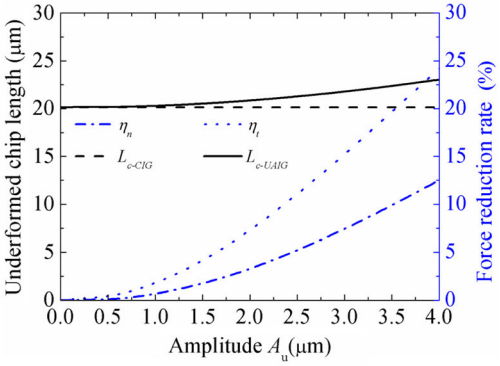

(d) Influence of UV amplitude A_u
(n_g=4000rpm, n_w=300rpm, V_c=10μm/min, f_o=0.625Hz)

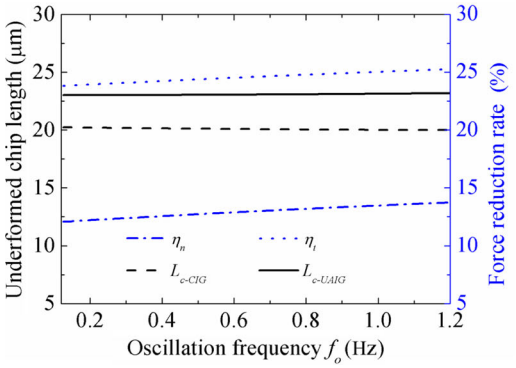

(e) Influence of oscillation frequency f_o
(n_g=4000rpm, n_w=300rpm, A_u=4m, V_c=10μm/min)

Fig. 11 Comparison between the underformed chip length and the force reduction rate for different process parameters

Subsequently, to explore the influences of the input variables on the grinding forces, CIG and UAIG tests were performed under different input variables and the grinding forces at t_0=75 s were picked up. As a result, Fig. 9 shows the influences of the input variables V_c, n_g, n_w, A_u, and f_o on the grinding forces in UAIG and CIG predicted using Eqs. (19) and (20) and obtained experimentally. Obviously, the variation tendencies and the quantitative values of the predicted forces also agree well with those of the experimental ones, regardless of the input variables either in CIG or in UAIG. It is also found from Fig. 9 that the grinding forces increase with the increasing of n_w and V_c, but decrease with the increasing of

n_g, A_u, and f_o; the influences of n_g, n_w, and V_c are strong, whereas that of A_u and f_o are significantly weak. Furthermore, it is noticed that the forces in UAIG are significantly smaller than those in CIG, meaning the presence of the UV affects the grinding forces significantly. It is inferred from Eqs. (19) and (20) that the shorter the undeformed chip length $L_{c\text{-}UAIG}$ or $L_{c\text{-}CIG}$ is, the larger the grinding forces become. The undeformed chip lengths $L_{c\text{-}UAIG}$ in UAIG and $L_{c\text{-}CIG}$ in CIG were calculated with Eq. (11) for various input variables as shown in Fig. 10. It is evident that the values of $L_{c\text{-}UAIG}$ in UAIG are larger than those of $L_{c\text{-}CIG}$ regardless of the input variables, indicating the reason why the grinding forces in UAIG are smaller than those in CIG can also be ascribed to the longer undeformed chip lengths in UAIG. Figure 10 shows SEM images of work surface finished by CIG and UAIG at n_w= 300 rpm, n_g=4000 rpm, V_c=10 μm/min, A_u=0/4 μm, f_u= 40 kHz, A_o=4 mm, and f_o=0.625 Hz. It is found that the cutting trace appears straight in the CIG while it is sinusoidal in the UAIG, indicating that the undeformed chip lengths is longer in UAIG than those in CIG. This confirmed that the reason why the grinding forces are reduced in UAIG compared to those in CIG is ascribed to the longer undeformed chip lengths in UAIG.

To evaluate the effect of UV on the grinding forces, force reduction rates were defined as $\eta_n=(1-F_{n\text{-}UAIG}/F_{n\text{-}CIG})\times 100$ (%) and $\eta_t=(1-F_{t\text{-}UAIG}/F_{t\text{-}CIG})\times 100$ (%) for normal and tangential forces, respectively. The values of η_n and η_t were obtained for different input variables using Eqs. (19) and (20) as shown in the same figure with the undeformed chip length, i.e., Fig. 11. Evidently, the η_n and η_t decrease with the increasing of n_g, n_w, and V_c, whereas increase with the increasing of A_u and f_o. In the other words, the effect of UV on the grinding force reduction can be enhanced with the decreasing of n_g, n_w, and V_c, but increasing of A_u and f_o.

5 Conclusion

In this study, a grinding force model for UAIG of SiC ceramics has been developed. The model incorporates many principal input variables (namely the workpiece rotational speed n_w, the wheel infeed rate V_c, the wheel rotational speed n_g, the UV amplitude A_u, and the oscillation frequency f_o) of the grinding process. Comparing the forces predicted using the developed model with the experimental ones shows that the variation tendencies and the quantitative values of the predicted forces agreed reasonably with those of the experimental ones. Relationships between the input variables and the grinding forces in UAIG can be concluded as follows:

1. The grinding forces are reduced in the UAIG compared to CIG, which is attributed to the formation of the longer undeformed chip length in the UAIG.
2. The grinding forces increase with the increasing of n_w and V_c, whereas decrease with the increasing of n_g, A_u, and f_o; the influence of n_g, n_w, and V_c on grinding force are much pronounced, whereas that of A_u and f_o are not very noticeable.
3. The force reduction of UV can be enhanced either by decreasing n_g, n_w, and V_c or increasing A_u and f_o.

This model can be reliably used for predicting the grinding forces in UAIG of SiC ceramics. It also can be severed as a useful springboard for development of more sophisticated UV assisted cutting force models.

Acknowledgments The present work was supported by the Fundamental Research Funds for the Central Universities. Authors thank Kimura Co., Ltd. for providing the SiC specimen used in experiments.

References

1. Nomura M (2007) Study of ultrasonic vibration assisted internal grinding of small holes. Doctoral Dissertation, Tohoku University
2. Peng Y, Wu YB, Liang ZQ, Guo YB, Lin X (2011) An experimental study of ultrasonic vibration-assisted grinding of polysilicon using two-dimensional vertical workpiece vibration. Int J Adv Manuf Technol 54(9–12):941–947
3. Peng Y, Liang Z, Wu Y, Guo Y, Wang C (2012) Effect of vibration on surface and tool wear in ultrasonic vibration-assisted scratching of brittle materials. Int J Adv Manuf Technol 59(1–4):67–72
4. Peng Y, Liang Z, Wu Y, Guo Y, Wang C (2012) Characteristics of chip generation by vertical elliptic ultrasonic vibration-assisted grinding of brittle materials. Int J Adv Manuf Technol 62(5–8): 563–568
5. Junichiro K, Yoshihisa I (1961) Study on ultrasonic internal grinding by using the longitudinally vibrated grinding wheel: 2nd report, the outline of the effects. Trans Jpn Soc Mech Eng 27(181):1412–1418
6. Wu Y, Nomura M, Kato M, Tachibana T (2003) Fundamental investigation of internal ultrasonic vibration assisted grinding of small holes. Proceedings of International Conference on Leading Edge Manufacturing in 21st century : LEM21, 2003: 145–150
7. Fujimoto M, Wu Y, Cao J (2011) High Precision Ultrasonically Assisted Internal Grinding (UAIG) of Difficult-to-machining Materials using Metal Bonded Diamond Wheels, Proceedings of The 6th International Conference on Leading Edge Manufacturing in 21st Century, Saitama, Japan, 2011
8. Cao Jianguo, W Yongbo, L Dong, Fujimoto M, Mitsuyoshi N (2014) Fundamental machining characteristics of ultrasonic assisted internal grinding of SiC ceramics. Mater Manuf Process 29(5):557–563
9. Cao Jianguo, W Yongbo, L Dong, Fujimoto M, Mitsuyoshi N (2014) Material removal behavior in ultrasonic-assisted scratching of SiC ceramics with a single diamond tool. Int J Mach Tools Manuf 79:49–61
10. Nomura Mitsuyoshi W, Yongbo KM, Toru T, Tsunemoto K (2005) Study of internal ultrasonic vibration assisted grinding of small

bore: mechanism of grinding force reduction due to ultrasonic vibration. J Jpn Soc Abras Technol 49(12):691–696 (In Japanese)
11. Keita S, Takumi T, Nobuhito Y, Jiwang Y, Tsunemoto K (2009) Ultrasonic-assisted micro-grinding with electroplated diamond wheels. J Jpn Soc Abras Technol 53(1):45–48 (In Japanese)
12. Qin N, Pei ZJ, Treadwell C, Guo DM (2009) Physics-based predictive cutting force model in ultrasonic-vibration-assisted grinding for titanium drilling. J Manuf Sci Eng 131(4):041001-1–041001-9
13. Yan W, Bin L, Xiaofeng Z (2014) Research on the system matching model in ultrasonic vibration-assisted grinding. Int J Adv Manuf Technol 70(1–4):449–458
14. Kun L, Warren L (1997) Modelling of ceramic grinding processes Part I. Number of cutting points and grinding forces per grit. J Mater Process Technol 65(1):1–10
15. Syoji K (2004) Grinding manufacturing. Yokendo, Tokyo
16. Arfken G (1984) University physics. Academic, Massachusetts
17. Sanjay A, Venkateswara RP (2013) Predictive modeling of force and power based on a new analytical undeformed chip thickness model in ceramic grinding. Int J Mach Tools Manuf 65:68–78